NMR investigations of medium-range order and quasicrystal formation in $Zr_{59}Cu_{20}Al_{10}Ni_8Ti_3$ metallic glass

H. Breitzke* and K. Lüders
Fachbereich Physik, Freie Universität Berlin, Arnimallee 14, D-14195 Berlin, Germany

S. Scudino, U. Kühn, and J. Eckert†
IFW Dresden, Institut für Metallische Werkstoffe, Helmholtzstr. 20, D-01069 Dresden, Germany
(Received 30 May 2003; revised manuscript received 11 March 2004; published 12 July 2004)

The structure and quasicrystal formation in bulk metallic glass-forming $Zr_{59}Cu_{20}Al_{10}Ni_8Ti_3$ are studied by means of nuclear magnetic resonance (NMR). The samples are prepared by rapid solidification and annealed to induce primary quasicrystal formation. ^{27}Al and ^{63}Cu NMR spectra and relaxation curves are recorded before and after the annealing process. Structure estimation is done by simulations of the second moments of various binary Al and Cu compounds. The Al spin-lattice relaxation time (T_1) of the order of 500 ms indicates a pseudogap in the density of states (DOS) at the Fermi level at Al sites similar as predicted by band structure calculations for binary AlZr compounds. Simulations of the second moments of various Al and Cu structures also favor the existence of binary L_{12} $AlZr_3$ and $C11_b$ $CuZr_2$ medium-range ordered regions in the metallic glass. The crystallization significantly changes the ^{63}Cu spectra and leaves the ^{27}Al spectra almost unchanged. The second moment of ^{63}Cu is strongly decreased after the crystallization accompanied by a strong increase in the ^{63}Cu spectral intensity. This indicates the formation of an icosahedral order involving CuX crystalline approximants.

DOI: 10.1103/PhysRevB.70.014201 PACS number(s): 71.23.Cq, 71.23.Ft, 76.60.−k

I. INTRODUCTION

Zr-based bulk glass-forming alloys are becoming more and more interesting candidates for industrial applications. These materials offer high strength-to-weight ratios and hardness as well as extreme springiness.[1,2] The superior properties of these new metals arise from the lack of a crystalline structure usually found in conventional metals and alloys. Moreover, Zr-based metallic alloys, for example, have the capability of forming quasicrystals by casting[3] or after heat treatment at approximately 700 K,[5,6] which can further improve the strength of the material.[7,8] However, these alloys are becoming very brittle after forming quasicrystals in the first step of crystallization. It is, therefore, of high importance to control the amount of crystallization within the metallic glass during the fabrication process. Their amorphous nature, however, makes their internal structure inaccessible for investigations by means of X-ray diffraction and other methods which require distinct long-range order within the material. $Zr_{59}Cu_{20}Al_{10}Ni_8Ti_3$, for example, yields in the glassy state a structureless X-ray diffraction pattern, consistent with its glassy nature.[8] After heat treatment the signature of an icosahedral symmetry arises in the diffraction pattern, indicating icosahedral ordering. The question whether the quasicrystal is formed during the heat treatment or is already present in the glassy state as nanocrystallites or quenched-in icosahedral clusters, which grow upon annealing, cannot be answered by X-ray diffraction.

Nuclear magnetic resonance (NMR), however, provides a local probe and is, therefore, a well-suited investigation method for obtaining information about crystalline phases or local atomic arrangements within a glass. Recently Tang *et al.*[4] have studied the crystallization process in $Zr_{41.2}Ti_{13.8}Cul2.5Ni10.0Be22.5$ bulk metallic glass by ^9Be NMR and were able to estimate the amount of Be that crystallizes in $BeZr_2$ during the crystallization process by investigating the ^9Be spin-lattice relaxation times.

Even though NMR is a local probe it requires a minimum of medium-range order if it is done on quadrupole nuclei like ^{27}Al and $^{63/65}Cu$. Otherwise the resonance frequency of quadrupole nuclei will be spread over a wide frequency range of several MHz due to a wide distribution of electrical field gradients (EFG) within the sample. As demonstrated by previous NMR measurements on the metallic glass $Zr_{55}Cu_{30}Al_{10}Ni_5$[9] the required short-range order is present in this compound and should be present in other metallic glasses as well.

The information about the local environment is in solid state NMR mainly obtained through the quadrupole interactions and through the hyperfine interactions, namely the electronic interaction and the dipole-dipole interaction. Pure metals like Al and Cu possess a high DOS leading to short spin-lattice relaxation times (T_1) of the order of ms, large Knight shift, large dipole-dipole interaction and no quadrupole interactions due to their cubic symmetry. For binary Al and Cu compounds like $AlZr_3$, which we assume to form in the investigated Zr-glasses, low DOS and, therefore, long T_1 are expected from band structure calculations.[10] The same NMR parameters are expected for the quasicrystal from previous NMR studies on single crystalline quasicrystals.[11] Quasicrystals possess a wide distribution of electric-field gradients (EFG), vanishingly small Knight shifts, consistent with large spin-lattice relaxation times and low DOS (pseudogap) at the Fermi level. In view of this and in order to obtain information about the crystalline and quasicrystalline phases, in this work a detailed investigation of the NMR

quadrupole and dipole-dipole interactions is done together with investigating and simulating the dipole-dipole interaction of various Al and Cu compounds before and after annealing the samples to the first crystallization peak.

II. EXPERIMENT

An ingot of nominal composition $Zr_{59}Cu_{20}Al_{10}Ni_8Ti_3$ was prepared by arc melting in a high purity argon atmosphere of 99.9999% purity. From this alloy ingot, ribbons with a cross-section of about 0.05×3 mm^2 were prepared by using the single-roller melt-spinning technique in a purified argon atmosphere.

The thermal behavior was measured by differential scanning calorimetry (DSC) using a Perkin-Elmer DSC 7 calorimeter in a flowing argon atmosphere at a heating rate of 40 K/min. For the annealing treatment of the samples, pieces of the ribbon were constant-rate heated to 742 K in the DSC. The structure of the as-prepared and annealed samples was analyzed by x-ray-diffraction (XRD) with Cu Kα radiation using a Philips PW 1050 diffractometer.

All NMR measurements were performed at 300 K in a magnetic field of $B \approx 13.83$ T with a phase coherent pulse spectrometer.

The spectra were recorded with a point by point method by changing the irradiation frequency in 20 kHz steps. A two pulse Hahn spin echo sequence was used for the detection of the xy magnetization. ^{27}Al and $^{63/65}$Cu spin-lattice relaxation times were measured in the central transition by employing the method of saturation recovery. A saturating pulse sequence of a duration τ longer than the T_1 time constant was applied in order to achieve high saturations.

Spin-spin relaxation was measured by enlarging the time spacing of the pulses of the spin echo sequence.

After completing the NMR measurements the sample was removed from the spectrometer and heated up to the temperatures of the first crystallization peak. Subsequently, all measurements were repeated on the heated sample.

III. RESULTS

A. Phase formation and thermal stability

Figure 1 shows the DSC curve of the as-quenched $Zr_{59}Cu_{20}Al_{10}Ni_8Ti_3$ ribbon. The sample exhibits a glass transition at $T_g = 660$ K, followed by three exothermic reactions with onsets $T_{X1} = 736$ K, $T_{X2} = 748$ K, and $T_{X3} = 764$ K, indicating a successive partial or complete transformation into different phases. To check the phase precipitated upon heating to the first transformation step, the as-quenched ribbon was heated to the temperature above the respective DSC peak, cooled to room temperature at a rate of 100 K/min and, subsequently, characterized by x-ray diffraction at room temperature.

Figure 2(a) shows the x-ray diffraction pattern of the as-quenched specimen and (b) displays the XRD pattern after heating to 742 K, respectively. The XRD for the as-quenched state ribbon in Fig. 2(a) shows no sharp crystalline peaks indicating an amorphous state. In contrast, Fig. 2(b) reveals a diffraction pattern which is typical for icosahedral order and

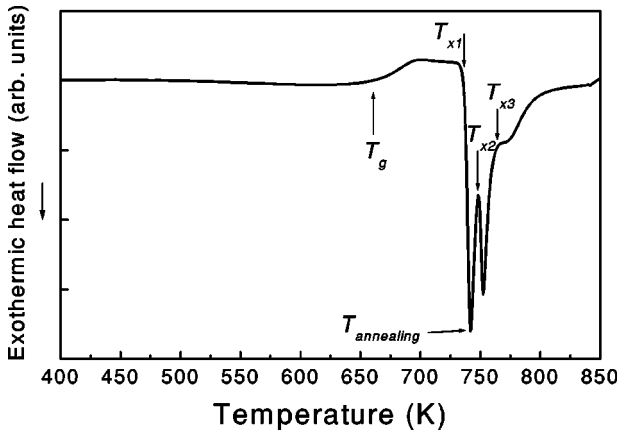

FIG. 1. DSC curve of the as-quenched ribbon of the $Zr_{59}Cu_{20}Al_{10}Ni_8Ti_3$ alloy. $T_g = 660$ K denotes the glass transition. The three exothermic reactions are denoted by the onsets $T_{X1} = 736$ K, $T_{X2} = 748$ K, and $T_{X3} = 764$ K.

is indexed in a notation following the indexing scheme of Bancel *et al.*[12]

B. Al and Cu NMR spectra

The ^{27}Al and ^{63}Cu spectra recorded before and after the annealing process are shown in Fig. 3. The ^{27}Al spectrum shows a central peak with two symmetric wings which are smeared quadrupole satellite transitions as it will be demonstrated by the simulation of the ^{27}Al spectra and have been observed by various authors in glassy alloys and single-phase quasicrystalline compounds.[11,13,14]

The ^{63}Cu spectrum shows no significant structure and is relatively low in intensity compared to the ^{27}Al spectrum. The reason for the low Cu spectral intensity is probably structural disorder within the Cu environment. The resonance frequencies of nuclei with quadrupole moments are sensitive to mechanical stress within a structure due to the coupling of the quadrupole moments to electrical field gradients in the vicinity of the nuclei. In diluted Cu and Al alloys, for ex-

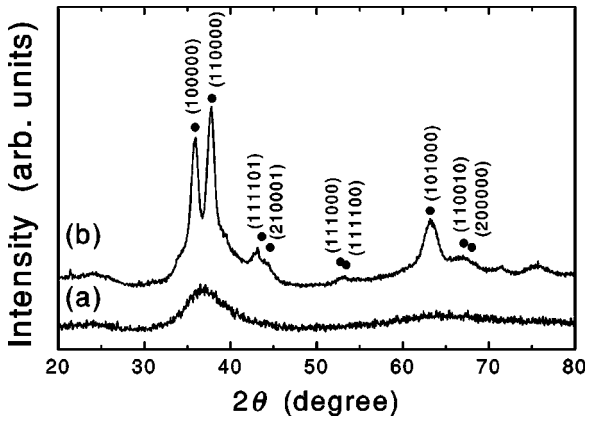

FIG. 2. X-ray diffraction pattern of the as-quenched $Zr_{59}Cu_{20}Al_{10}Ni_8Ti_3$ glassy ribbon (a), and after annealing at the peak temperature of the first crystallization event (b). The sample was heated to 742 K.

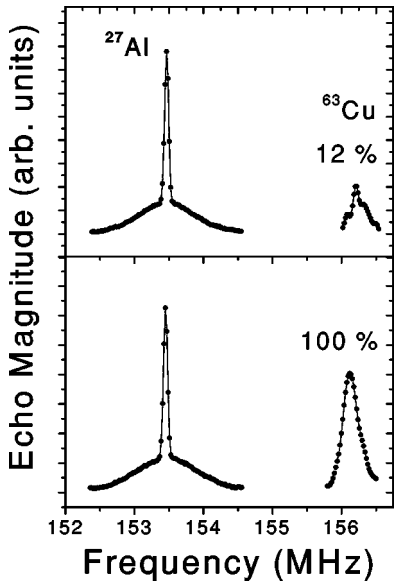

FIG. 3. ^{27}Al and ^{63}Cu NMR spectra before (upper picture) and after (lower picture) heating the sample to the first crystallization peak. The solid lines are guides to the eyes.

ample, an amount of only a few percent dopants is sufficient to achieve a striking decrease of the signal intensity by almost two orders of magnitude.[15,16]

From the existence of relatively well-structured NMR spectra one can conclude the existence of structured regions within a material. This assumption is supported by strongly different T_1 of ^{63}Cu and ^{27}Al indicating strongly different DOS at Cu and Al sites, which is discussed in Sec. III E 2. Because the x-ray diffraction pattern does not show sharp Bragg peaks these regions have to be only a few nm in size.

No significant changes in the ^{27}Al spectra are recorded after heating the sample to the first crystallization peak. In the ^{63}Cu spectrum, however, two remarkable changes can be observed. The intensity of the ^{63}Cu spectrum strongly increases, due to reordering of the Cu environment and the center frequency of the spectrum is slightly shifted to lower frequencies. Thus, annealing the sample mostly affects the Cu environment indicating that rearrangement of Cu atoms is directly involved in the quasicrystal formation whereas the environment of Al atoms remains almost unchanged.

The Al environment, however, is not completely unaffected by the crystallization. It might be slightly compressed due to the quasicrystal formation as it will be demonstrated by the simulation of the ^{27}Al spectra and by the second moments which are utilized for the structural estimations of the ^{27}Al and $^{63/65}$Cu environments and their changes during the crystallization process.

C. Simulations of the ^{27}Al NMR spectra

The ^{27}Al line shape is typical for nuclei with $I>1/2$ in an environment like metallic glasses or quasicrystals.[11,13,14] The central peak of the ^{27}Al spectrum arises from the $|\pm\frac{1}{2}\rangle$ transition whereas the broad wings besides the central peak arise from the quadrupole interaction.

^{27}Al and $^{63/65}$Cu nuclei have sizeable quadrupole moments. In a structure with noncubic symmetry placed in a magnetic field the total Hamiltonian of a quadrupole nucleus may be written $H_Z+H_{\mathrm{quad}}+H_{\mathrm{mag}}$, where H_Z denotes the Zeeman energy, arising from the coupling of the nuclei to the static magnetic field, H_{quad} denotes the coupling of the quadrupole moment to the electric field gradient (FEG) and H_{mag} describes the hyperfine interactions of the nuclear moment with the electronic environment.[17,18]

In general, the eigenvalues of the quadrupole and hyperfine interactions depend on the orientation of the static magnetic field with respect to the EFG's and hyperfine interaction tensors. For the case where $H_Z \gg H_{\mathrm{quad}}, H_{\mathrm{mag}}$ the parts H_{quad} and H_{mag} may be treated as perturbations and the transition frequency may be written in the form $\omega=\omega_Z+\omega_{\mathrm{quad}}+\omega_{\mathrm{mag}}$. The first term $\omega_Z=\gamma B_0$ denotes the Zeeman transition and the hyperfine interaction ω_{mag} may be written in first order as[19,20]

$$\omega_{\mathrm{mag}}=\omega_Z\left(K_{\mathrm{iso}}+\frac{K_{\mathrm{aniso}}}{2}(3\cos^2\theta-1)-\frac{\varepsilon K_{\mathrm{aniso}}}{2}\sin^2\theta\cos 2\phi\right), \tag{1}$$

with $K_{\mathrm{iso}}=\frac{1}{3}(K_x+K_y+K_z)$, $K_{\mathrm{aniso}}=K_z-K_{\mathrm{iso}}$ and K_i as the components of the hyperfine interaction tensor in the principal-axis system and $\varepsilon=(K_y-K_x)/K_{\mathrm{aniso}}$. The quadrupole shift in first order may be written[19,20]

$$\omega_{\mathrm{quad}}=\frac{\omega_Q}{2}\left(m-\frac{1}{2}\right)(3\cos^2\theta-1-\eta\cos 2\phi\sin^2\phi), \tag{2}$$

with $\omega_Q=3e^2qQ/2I(I+1)h$ as the quadrupole frequency, $eq=V_{zz}$ as z-component of the EFG tensor, $\eta=(V_{xx}-V_{zz})/V_{zz}$ as the asymmetry parameter and θ, ϕ as the Euler angles between the principal axis and the static magnetic field B_0. The Larmor frequency $\omega_0=\gamma B$ is set positive.

In second order the quadrupole interaction affects the central transition and the second order shift of the $|\pm\frac{1}{2}\rangle$ transition for the case $\eta=0$ may be written as[18]

$$\omega_{1/2}=\frac{-\omega_Q^2}{16\omega_Z}\left(I(I+1)-\frac{3}{4}\right)(1-\cos^2\theta)(9\cos^2\theta-1). \tag{3}$$

In long-range ordered systems the EFG and hyperfine tensors are determined by the crystal symmetry. In glassy alloys, however, only short-range order exists and one can hardly speak about an unified principal axis system for both tensors. For the simulations, it is therefore assumed that both tensors are independent from each other.

The width of the wings besides the ^{27}Al central transition is of the order of 1 MHz with respect to the central transition peak frequency indicating a first order quadrupole splitting. Because the first order quadrupole splitting affects only the satellite transitions $|\pm\frac{5}{2}\rangle\rightarrow|\pm\frac{3}{2}\rangle$ and $|\pm\frac{3}{2}\rangle\rightarrow|\pm\frac{1}{2}\rangle$ the Gaussian-type broadening of the central transition in Fig. 5 arises from a distribution of the hyperfine interaction tensors. The contribution to the broadening of the central transition due to the quadrupole interaction can be estimated to of the order of only 2 kHz. Consequently, a Gaussian-type distribution of K_{iso} is assumed for the simulations. In addition, a

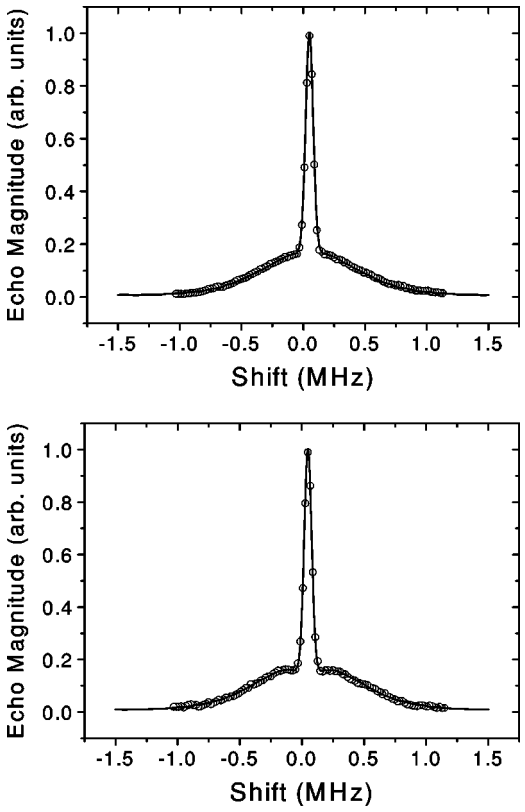

FIG. 4. Simulation (solid line) of the ^{27}Al NMR spectra before (upper picture) and after (lower picture) the heating to the first crystallization peak. The parameters used in the simulation are ω_Q =0.68 MHz, $\overline{\omega_Q}$=0.2 MHz , K_{iso}=50 kHz, $\overline{K_{\mathrm{iso}}}$=30 kHz η=0.6, $\overline{\eta}$ =0.3…0.9 for the upper picture and ω_Q=0.868 MHz, $\overline{\omega_0}$ =0.192 MHz, K_{iso}=50 kHz, $\overline{K_{\mathrm{iso}}}$=30 kHz η=0.4, $\overline{\eta}$=0.1…0.7 for the lower picture.

Gaussian-type distribution of the quadrupole interaction parameters η, ω_Q is assumed, according to NMR spectra simulations for ^{27}Al NMR spectra of quasicrystals by Shastri *et al.*[11] All simulations were performed with the SIMPSON solid-state NMR simulation package, which is described in Ref. 21.

The parameters used in the simulations are denoted ω_Q for the quadrupole frequency, $\overline{\omega_0}$ for the standard deviation of the frequency distribution, K_{iso} for the isotropic hyperfine interaction, $\overline{K_{\mathrm{iso}}}$ for it's standard deviation and η for the EFG's anisotropy parameter and $\overline{\eta}$ for the distribution of η values in steps of 0.1.

Because the simulated spectra are less sensitive to the variation of the asymmetry parameter and in order to save calculation time the η value was increased in steps of 0.1. In all calculations K_{aniso} was set zero and the line broadening was set to a value according to the measured spin-spin relaxation time T_2.

The results of the powder pattern simulations are shown in Fig. 4 together with the used as parameters listed in the figure caption of Fig. 4.

1. Quadrupole interaction

A good agreement between the simulations and measurements can be achieved for a distribution of the quadrupole frequency of 0.52 MHz with a center frequency of 1.68 MHz. After the crystallization an increase of the quadrupole frequency of 0.48 MHz can be recorded together with a slight decrease of its standard deviation accompanied by a decrease of the asymmetry parameter. It is remarkable that after the crystallization the quadrupole interaction has significantly increased by 30% whereas the width of the ^{27}Al central transition remains constant. It will be shown in section (13) that the ^{27}Al second moment is also significantly increased by 50% after the crystallization indicating that the EFG is dominated by the lattice EFG produced by lattice charges.

The net EFG is in general the sum of the lattice EFG that is produced by the lattice ions, enhanced by the Sternheimer antishielding γ_∞ and a conduction electron contribution:[22]

$$eq_{\mathrm{net}} = eq_{\mathrm{lat}}(1 - \gamma_\infty) - eq_{ce}. \tag{4}$$

In terms of spherical coordinates the EFG in z-direction produced at the origin by a point charge at a distance r may be expressed as:

$$eq_{zz} = e\frac{(3\cos^2\theta - 1)}{r^3}. \tag{5}$$

The dipole-dipole interaction exhibits also $1/r^3$ dependency. Hence, an increase of the quadrupole interaction accompanied by an increase of the second moment at comparable rates is a strong hint for a dominant lattice part in Eq. (4), since a decrease of the average distance r of the nuclei will influence both quantities at the same rate and has negligible influence on the width of the central transition. The order of magnitude of the distribution of lattice positions within the Al environment can now roughly be estimated by utilizing Eq. (5). Setting e to one, θ to zero and using a Gaussian-type distribution of r with mean value one and standard deviation 0.06 yields a Gaussian-type distribution of eq_{zz} with a standard deviation of 0.20. This rate is of the order of the standard deviation of the quadrupole interaction rate used for the ^{27}Al spectra simulation and will be introduced into the simulations of ^{27}Al second moments in Sec. IV B.

2. Knight shift

The Knight shift at the center of the ^{27}Al transition is of the order of 0.03% and is approximately five times smaller than the Knight shift reported for pure metallic aluminium.[23] The measured value is, however, consistent with ^{27}Al Knight shift values reported for trialuminide intermetallics[24,25] indicating a low DOS at the Fermi level. The width of the central transition has to be due to Knight shift distributions attributed to disorder in the Al environment and size effects.[26]

D. Cu spectra

The interpretation of the ^{63}Cu spectra is more difficult than the interpretation of the ^{27}Al spectra. From the ^{63}Cu spin-lattice relaxation it is clear that a quadrupole interaction is present (Fig. 6). The signal-to-noise ratio (SNR) at 300 K, however, is to poor to record the satellite transition in an appropriate time. Cooling the sample will strongly increase

the SNR and the quadrupole transitions can be recorded. At 30 K the ^{63}Cu spectrum (not shown here) has a structure similar to the ^{27}Al spectra, but with strongly smeared-out wings. A reliable estimation of the quadrupole interaction can hardly be given, because the completely smeared-out quadrupole transitions vanish smoothly in the noise without any kink. Very roughly estimated a quadrupole frequency of the order of 4 MHz is necessary for the recorded negative shift. Nevertheless, one can estimate the amount of ^{63}Cu that is visible in the spectra by comparing the intensity obtained from fitting a Gaussian to the ^{63}Cu spectrum to the intensity obtained from a respective fit to the ^{27}Al central transition. Assuming that the ^{63}Cu spectrum before the crystallization can be attributed to a $CuZr_2$ alike structure one obtains a value of 12% visible ^{63}Cu before the crystallization and nearly 100% after the crystallization, indicating a strong reordering of the Cu environment.

E. Spin-lattice relaxation

1. ^{27}Al *spin-lattice relaxation*

If quadrupole interaction is involved, the spin-lattice relaxation is no longer of a single exponential form, as for the simple case of $I=\frac{1}{2}$ nuclei. The quadrupole interaction changes the level spacing resulting in unequally spaced multi-level systems. In order to predict the correct form of the relaxation curve one has to know the dominant relaxation mechanism.[27] For metals the dominant relaxation mechanism is in general magnetic. In that case and for $I=\frac{5}{2}$ nuclei the spin-lattice recovery law for long saturation times may be written as[27–29]

$$M(t) = M(\infty)\left(1 + 0.257\ \exp\left(\frac{-2t}{T_1}\right) + 0.267\ \exp\left(\frac{-12t}{T_1}\right) + 0.476\ \exp\left(\frac{-30t}{T_1}\right)\right). \quad (6)$$

For $I=\frac{3}{2}$ nuclei the corresponding recovery law may be written

$$M(t) = M(\infty)\left(1 + 0.4\ \exp\left(\frac{-2t}{T_1}\right) + 0.6\ \exp\left(\frac{-12t}{T_1}\right)\right). \quad (7)$$

Long saturation should be understood as a saturating time longer than the relaxation time T_1.

Fitting the relaxation curves with Eq. (6) results in reasonable well agreement between the measurements and the recovery laws (Fig. 5). Note, that although the recovery laws are composed of three exponential functions, the fits have only two free parameters.

The spin-lattice relaxation time $T_1=590(20)$ ms is exceedingly long for metallic compounds, giving a reliable indicator of a gap in the density of states (DOS) at the Fermi level as predicted for binary metallic compounds like $AlZr_3$.[10] The significant reduction of the spin-lattice relaxation time to $T_1=362(15)$ ms after the crystallization may indicate a change of the Fermi level due to the formation of the quasicrystal. It does not necessarily indicate a complete change in the Al environment.

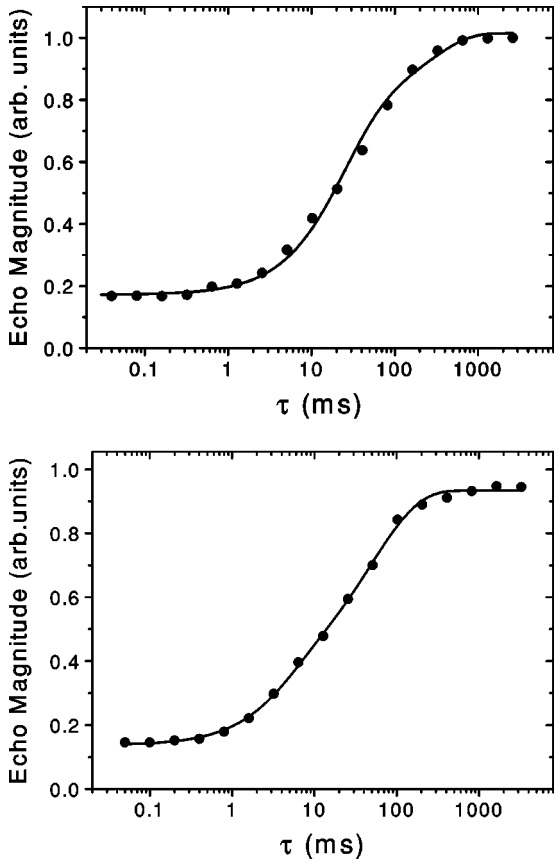

FIG. 5. Semi-logarithmic plot of the normalized nuclear magnetization recovery curves of the ^{27}Al central transition following a long saturating pulse sequence. The relaxation times obtained from the fits (solid lines) are 590(20)ms before the crystallization (upper picture) and 362(15)ms after the crystallization (lower picture).

The decrease of T_1 seems to be in contradiction to the constant Knight shift in the ^{27}Al spectra after the crystallization. Since T_1 is related to the Knight shift $\Delta\omega$ via the Korringa[30] relation

$$T_1(\Delta\omega)^2 = \frac{\hbar}{4\pi k_B T}\frac{\gamma_e^2}{\gamma_n^2}, \quad (8)$$

an increase of the Knight shift of approximately 13 kHz is expected from Eq. (8) from the recorded decrease of T_1 after the crystallization. However, calculating the expected Knight shift from the ratio of $T_1=6.3$ ms and $K_s=0.164\%$ reported for metallic aluminium[23] and the measured T_1 of 590 ms yields only half of the measured Knight shift, i.e., 28 kHz.

In general, the experimental values for T_1 are shorter than the predicted ones[23] and Eq. (8) represents only one contribution to the spin-lattice relaxation time: The coupling of magnetic moments of *s*-state electrons to the nuclei. Thus, further contributions to the Knight shift have to be present, larger than the Knight shift contribution from *s*-like states, for example a contribution from *d*-like states, orbital paramagnetism and core polarization as widely assumed for many metallic alloys.[24,25,31] Hence, the decrease in T_1 after

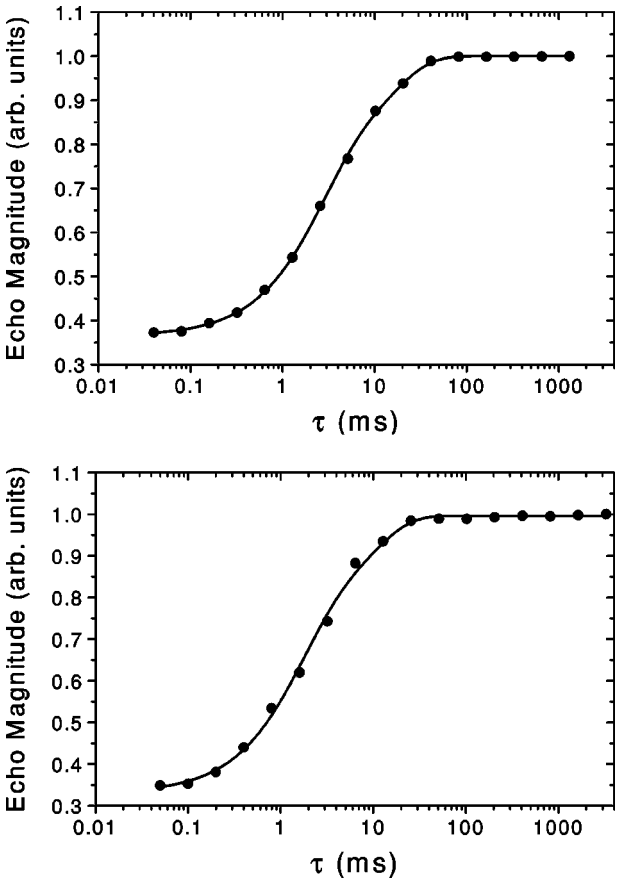

FIG. 6. Semi-logarithmic plot of the normalized nuclear magnetization recovery curves of the ^{63}Cu nuclei at the peaks of the spectra following a long saturating pulse sequence. The relaxation times obtained from the fits (solid lines) are 28.4(4) ms before the crystallization (upper picture) and 18.2(4) ms after the crystallization (lower picture).

the crystallization is not necessarily mirrored in the Knight shift.

2. ^{63}Cu *spin-lattice relaxation*

The ^{63}Cu spin-lattice relaxation curves and the fits using Eq. (7) are shown in Fig. 6. From the fits the following relaxation times are obtained: 28.4(4) ms before the crystallization and 18.2(4) ms after the crystallization. Again, a decrease of the T_1 after the crystallization as for the ^{27}Al spin lattice relaxation is observed.

In general the T_1 process in metals is driven by the coupling of the nuclei magnetic moments to the conduction electrons which leads to the Korringa relation (8). Including the DOS in an explicit form the Korringa relation (8) may be written as[17]

$$T_1(\Delta\omega)^2 = \left[\frac{\chi_e^s}{\varrho(E_F)}\right]^2 \frac{1}{\pi kT}\frac{1}{\gamma_n^2\gamma_e^2\hbar^3}, \tag{9}$$

with $\varrho(E_F)$ the DOS at the Fermi level and χ_e^s the electronic susceptibility. Since there is only one T_1 for ^{27}Al one can conclude that every ^{27}Al nuclei has the same DOS.

Band structure calculations for binary amorphous metallic alloys[32] show that the pronounced structure of the electronic DOS of the crystalline phase is smeared-out in an amorphous phase. Hence one can conclude that the gap at the Fermi level as calculated for $AlZr_3$ should be smeared-out and the ^{27}Al T_1 should be significantly shorter than the measured one. Furthermore, according to equation (9) $T_1(^{27}\mathrm{Al})$ and $T_1(^{63}\mathrm{Cu})$ should differ only by their γ ratio, i.e., by 2%. The first order quadrupole interaction does not change the situation in any essential way. However, the $T_1(^{27}\mathrm{Al})$ and $T_1(^{63}\mathrm{Cu})$ differ by a factor of 20. Such a large ratio can only be explained by distinct DOS at Al and Cu sites. Hence, Al and Cu must be incorporated into distinct medium-range ordered regions to achieve the required distinct densities of states.

After the crystallization the ^{63}Cu spectrum is shifted significantly to lower frequencies in contrast to the ^{27}Al spectra. Because of the decreased T_1 after the crystallization the spectra should be shifted to higher frequencies or remain at least at the same position in the spectrum. The negative shift can only be explained by an increased quadrupole interaction resulting in a second order shift of the central transition. According to Eq. (3) a second order shift is negative and may dominate all other contributions to the shift. Together with the strong increase of the ^{63}Cu spectral intensity a remarkable change in the Cu environment can be concluded. This conclusion will be verified by corresponding changes in the ^{63}Cu spin-spin relaxation curve as discussed in Sec. III G.

F. Spin-spin relaxation

1. ^{27}Al *spin-spin relaxation*

Spin-spin relaxation describes the loss of phase coherence of a spin ensemble. In solids such a coherence loss is mainly driven by dipolar couplings and fluctuating magnetic fields for example caused by the Fermi contact interaction in conductive solids which is an effective mechanism also for spin-lattice relaxation.[17] The Hahn spin echo sequence cancels out all static inhomogeneities, which may affect the Larmor frequency of a nucleus yielding a homogeneous line width determined by the lifetime of the exited states. The dipole-dipole interaction of like spins, however, will not be canceled out by the spin-echo and contributes to the line width. In the static limit $(T_2/T_{2G} \ll 1)$ the decoherence is described by the static dipolar interaction yielding a Gaussian line shape, which is described in the time domain by a Gaussian decay function[33,34]

$$M(2\tau) = M_0 \exp\left(-\frac{1}{2}\left(\frac{2\tau}{T_{2G}}\right)^2\right). \tag{10}$$

When the case is not static an exponential contribution from the decoherence process due to field fluctuations has to be taken into account (see, for example, Refs. 33 and 34), giving

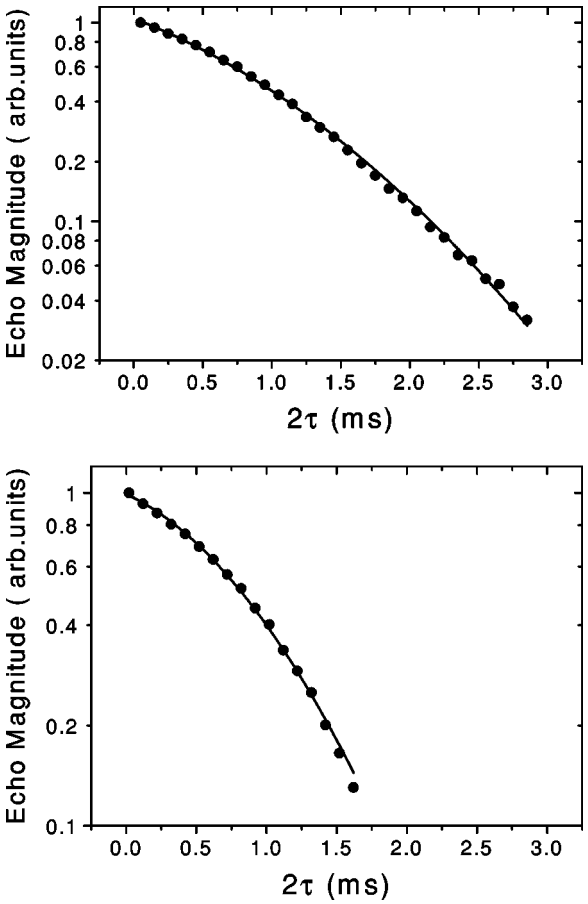

FIG. 7. Semi-logarithmic plots of the spin echo decays of the ^{27}Al central line. The relaxation times obtained from the fits of Eq. (11) to the data are $T_2=1.60(20)$ ms and $T_{2G}=1.50(2)$ ms before the crystallization (upper picture) and $T_2=2.00(20)$ms and $T_{2G}=1.00(2)$ ms after the crystallization (lower picture).

$$M(2\tau) = M_0 \exp\left(-\frac{2\tau}{T_2} - \frac{1}{2}\left(\frac{2\tau}{T_{2G}}\right)^2\right). \qquad (11)$$

In general, one has to take into account a contribution to the spin echo decay from T_1.[35] However, the measured T_1 and T_2 differ by two orders of magnitude and the contribution from T_1 can be neglected. The spin-spin relaxation curves of ^{27}Al are shown in Fig. 7. The upper figure shows the T_2 data before and the lower figure the T_2 data after the crystallization. A significant increase of T_2 can be seen. The data in both figures are fitted by the Eq. (11) with M_0, T_2, and T_{2G} as free parameters.

The data in both figures are fitted by the Eq. (11) with M_0, T_2, and T_{2G} as free parameters.

Utilizing the method of moments[17,18] gives a convenient representation of the dipole-dipole interaction by expressing it in terms of the second moment. The second moment represents the width of a resonance line and is best approximated by a Gaussian line shape. For the details see Refs. 17 and 18. The relaxation times obtained from the fits in Fig. 7 are listed in the figure caption of Fig. 7. A significant decrease of T_{2G} can be observed after the crystallization. Consequently, the average dipole-dipole distance must be reduced. This is consistent with the observed increase of the quadrupole frequency and may indicate either a structural change of the Al environment or a compression of the Al environment due to the quasicrystal formation. We will return to this point after the simulation of the second moments.

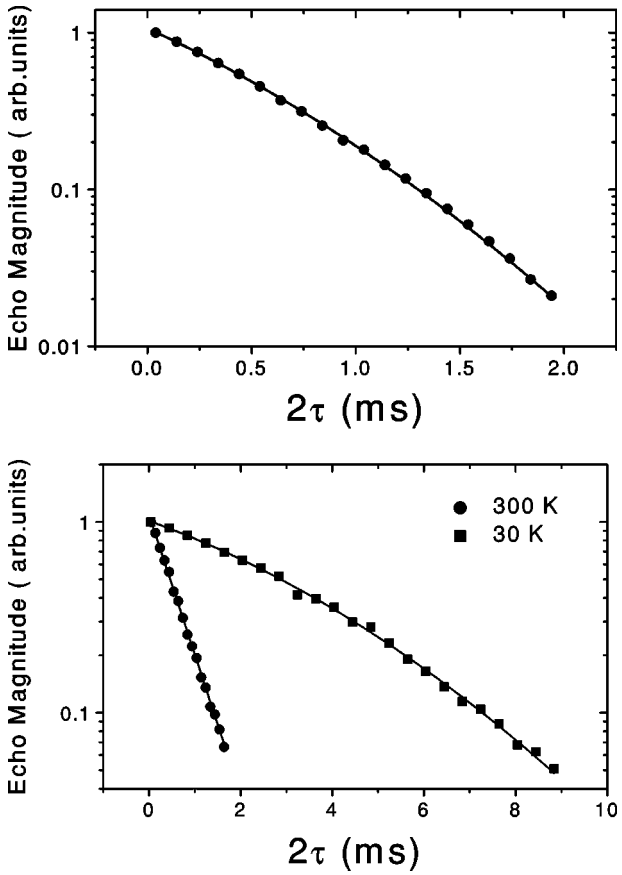

FIG. 8. Semi-logarithmic plot of the spin echo decay of the ^{63}Cu nuclei in the center of the spectrum before (upper picture) and after heat treatment (lower picture). The data in the upper picture are fitted by Eq. (11). The relaxation times obtained from this fit are $T_2=0.714(13)$ ms and $T_{2G}=1.24(4)$ms. The data in the lower figure are recorded after the crystallization at 300 K (circles) and 30 K (squares). The data at 300 K are fitted with a single exponential function obtaining a relaxation time of $T_2=0.580(1)$ ms. At 30 K the strongly enlarged T_2 of 5.1(1) ms reveals a Gaussian part of $T_{2G}=5.5(2)$ ms.

G. ^{63}Cu spin-spin relaxation

^{63}Cu spin-spin relaxation curves and corresponding fits are shown in Fig. 8.

Before the crystallization (upper picture) the relaxation curve possesses a Gaussian contribution. A fit with Eq. (11) yields the relaxation times $T_2=0.714(13)$ ms and $T_{2G}=1.24(4)$ ms. After the crystallization the Gaussian contribution has disappeared from the relaxation curve and a single exponential fit to the data yields the value $T_2=0.580(1)$ ms. The lack of the Gaussian contribution in the relaxation curve after the crystallization verifies the conclusion that a complete change of the Cu environment during the crystallization

process takes place. If one compares the changes in the ^{63}Cu spectra with the changes in the x-ray diffraction pattern obtained after the crystallization a quasicrystal formation involving CuX compounds can be concluded.

A disappearing of the Gaussian contribution in the spin-spin relaxation curve, however, does not necessarily mean complete disappearing of dipole-dipole interactions. Instead it is more probable that it has reduced during the crystallization and is merely covered by the T_2 process, the first part of Eq. (11).

The minimum value of T_{2G} that can be covered by a T_2 of 0.5 ms may be estimated to be of the order of 7 ms. This estimation is verified by the T_2 curve recorded at 30 K. The strongly enlarged T_2 at 30 K revealed a T_{2G} of 5.5(2) ms which is consistent with the above estimation if one takes into account the contraction of the lattice constants at 30 K.

IV. SIMULATIONS OF SECOND MOMENTS

In the presence of quadrupole interaction contributions from $|\pm\frac{3}{2}\rangle$ and $|\pm\frac{5}{2}\rangle$ states should be treated as contributions from unlike spins and canceled out by the Hahn echo sequence. However, analyzing the T_{2G} results in the case of a broad central transition and distributed quadrupole interaction is more complicated than in the case of the small and well separated lines of a single crystal. As mentioned above T_{2G} is measured with a Hahn spin echo sequence which is commonly understood as a pulse sequence attributed to $\pi/2$ and π tip angles. However, since only a small fraction of the central line is excited by the pulse sequence, the $\pi/2$ and π tip angles are found only around the center frequency of the excitation bandwidth that is within a small fraction of the whole excitation bandwidth. Nuclei excited beside the center frequency experience smaller tip angles. Furthermore, the central peak of the ^{27}Al spectrum contains considerable contributions from the $|\pm\frac{3}{2}\rangle$, $|\pm\frac{5}{2}\rangle$ states due to the distributed quadrupole interaction which are also excited by the spin echo sequence. For this reasons, the present conditions are much more complex as the conditions in the case of well defined single crystals where the central transition is well separated from the satellite transition and can be completely excited by a $\pi/2$ and π pulse sequence. Therefore, the present conditions require special theoretical analyzes that are not within the scope of this work.

In order to overcome this problem we followed a phenomenological way by analyzing the second moments in the way described by Abragam[18] and compared the calculated ^{63}Cu(T_{2G}) values with the experimental ones of a $CuZr_2$ reference sample. To correct deviations from the calculated and experimental values a phenomenological parameter may be introduced. However, the calculated ^{63}Cu(T_{2G}) value shows good agreement with the experimental value (Sec. IV A). The deviations are smaller than 6% within experimental accuracy.

The method of moments utilizes the fact that magnetic dipoles a distance r apart from each other produce a magnetic field of the order $B_{\mathrm{loc}}=\mu/r^3$. Expressed in terms of the second moment, the dipole-dipole interaction for like spins may be written as[17]

$$\langle \Delta\omega^2 \rangle = \frac{3}{4}\gamma^4\hbar^2 I(I+1)\sum_k \frac{(1-3\cos^2\theta_{jk})^2}{r_{jk}^6}, \qquad (12)$$

with the gyromagnetic ratio of the nuclei γ, the quantum spin number I and the dipole-dipole distance r_{ij}. In case of powder samples the angular-dependent part $(1-3\cos^2\theta_{jk})^2$ may be replaced by it's average value $4/5$. In general one should take into account a correction due to the presence of quadrupole interaction.[18] In the presence of quadrupole interaction the dipolar broadening of the $\pm 1/2$ transition can be divided into different cases: 1. like spins: Spins with the same gyromagnetic ratio and situated at crystal sites with the same EFG and 3. semi-like spins: Spins with the same gyromagnetic ratios but located at different sites and experiencing different quadrupole couplings.[18] In general, second moments in imperfect cubic crystals are calculated by the introduction of a coherence radius inside which the spins are treated as like spins and as semi-like outside.[18] The ratios r_L and r_{SL} of the second moments for like and semi-like spins to that without quadrupole coupling depend on I and are: $r_L(3/2)=9/10$, $r_{SL}(3/2)=4/5$, $r_L(5/2)=107/105$, and $r_{SL}(5/3)=257/315$.[18] The like spins within the coherence radius are most effective for the second moments and the T_{2G} is effected only by the square root of r_L and r_{SL}. Hence, the correction due to semi-like spins can be estimated to be smaller than 1% and and are expected to vanish within the experimental error, remaining only the correction for like spins which is about 5% for Cu. r_L can be neglected for Al. Therefore, only a small correction is applied to Eq. (12) for Cu nuclei. The expressions for T_{2G} may be written for aluminium:

$$T_{2G} = \sqrt{5.25\gamma^4\hbar^2\sum_k r_{jk}^{-6}}^{-1}, \qquad (13)$$

and for the copper nuclei:

$$T_{2G} = \sqrt{2.25\cdot r_L\gamma^4\hbar^2\sum_k r_{jk}^{-6}}^{-1}, \qquad (14)$$

T_{2G} for ^{63}Cu has to be corrected due to the natural abundance of the ^{63}Cu isotope. Contributions from ^{65}Cu will be cancelled out by the echo-sequence in the static limit ($T_1/T_2 \gg 1$)[33] and the sum in Eq. (14) will only count contribution from ^{63}Cu. Provided a stochastic distribution of both isotopes the ^{63}Cu T_{2G} will be enlarged by $1/\sqrt{0.7}$ with 0.7 as the natural abundance of ^{63}Cu which yields a T_{2G} of 1.54 ms for ^{63}Cu in $CuZr_2$. The validity of the above argumentation is confirmed by the ^{63}Cu second moment in a $CuZr_2$ reference sample. $CuZr_2$ possess a tetragonal structure, however, the quadrupole interactions is relatively weak ($\omega_Q=120$ kHz) and the ^{63}Cu NMR spectrum shows washed out satellite transitions (Fig. 10) indicating disorder within the $CuZr_2$ structure. From the NMR point of view the Cu in $CuZr_2$ may resembles an environment with slowly varying quadrupole interaction according to an disordered cubic environment. Hence, the treatment of ^{63}Cu second moments in $CuZr_2$ according to Eq. (14) is indicated.

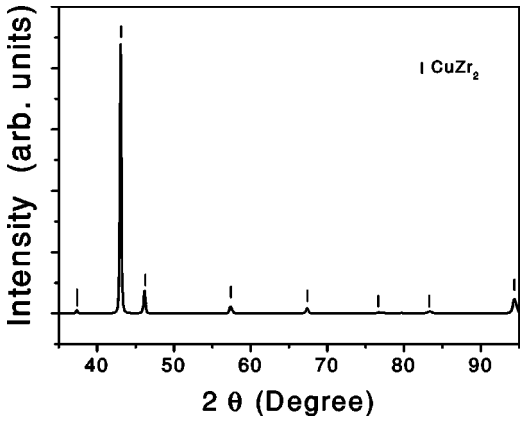

FIG. 9. XRD pattern of the annealed $CuZr_2$ sample.

A. $CuZr_2$ reference sample

The reference sample was prepared by using the single roller-melt spinning technique. The obtained ribbon was annealed at 673 K for 30 minutes and rapidly cooled down to room temperature. The existence of the $CuZr_2$ phase within the sample is clearly proofed by the XRD which is shown in Fig. 9.

From the tetragonal $C11_b$ structure of $CuZr_2$ quadrupole interaction and anisotropic chemical shift is expected for the ^{63}Cu NMR powder spectrum which is shown in Fig. 10.

Broadened peaks in the XRD pattern (Fig. 9) indicate imperfections in the crystal lattice that may wash out the satellite transitions in the NMR powder pattern. The solid line in Fig. 10 denotes the powder pattern simulation which was found to be the best approximation for the experimental spectrum. The satellites are washed out indeed due to slight disorder in the $CuZr_2$ crystallites.

The spin-lattice relaxation curve is shown in Fig. 11 and possess the double exponential form according to Eq. (7) as expected for the relaxation process in the presence of quadrupole interaction. A fit with Eq. (7) yields a value of T_1 = 16.0(4) ms which indicates the predicted gap at the Fermi level for binary metallic compounds like $AlZr_3$ and $CuZr_2$.[10] In general, the ^{63}Cu T_1 in pure $CuZr_2$ and $CuZr_2$ embedded in an amorphous alloy are not expected to be fully equal. According to Eq. (9) the T_1 depend on the DOS at the Fermi level which may be shifted due to the contact to the amorphous or medium-range ordered environment.

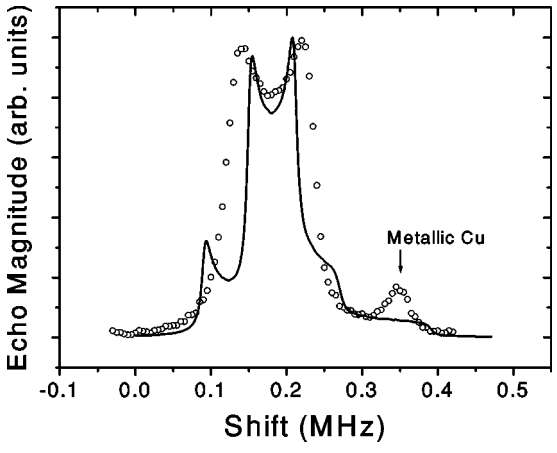

FIG. 10. Measured spectrum (open circles) and simulation (solid line) of the $CuZr_2$ reference sample. The parameters of the simulation are: ω_Q=120 kHz, K_{iso}=190 kHz, and K_{aniso}=80 kHz. The satellite transition are washed out due to crystal imperfections and the spectrum is slightly broadened.

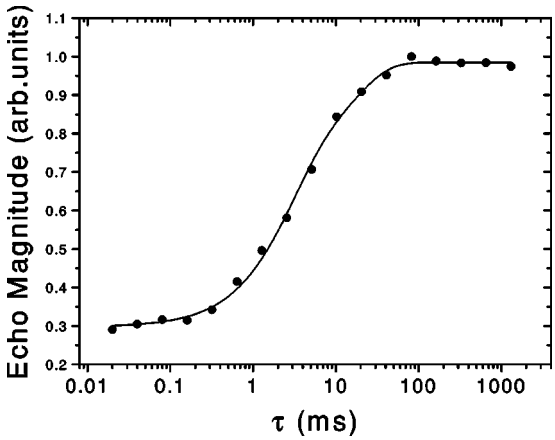

FIG. 11. Semi-logarithmic plot of the normalized ^{63}Cu nuclear magnetization recovery curves of the $CuZr_2$ reference sample measured at 150 kHz following a long saturating pulse sequence. The spin-lattice relaxation time obtained from the fit (solid line) is 16.0(4) ms.

The spin-spin relaxation curve is shown in Fig. 12. A fit with Eq. (11) obtains the value T_{2G}=1.44(4)ms which is in excellent agreement with the calculated value of $T_{2G} \approx 1.54$ ms for ^{63}Cu in $CuZr_2$. The small deviation is expected because the experimental T_{2G} is in general smaller than the theoretical one.[36] Experimental T_{2G} for metallic Al are about 10% smaller than the calculated value[36] and experimental and calculated T_{2G} for ^{63}Cu in $CuZr_2$ differ by the expected amount.

B. ^{27}Al second moments

Second moment calculations are in general only valid for large crystals because nuclei in outer shells or at the bound-

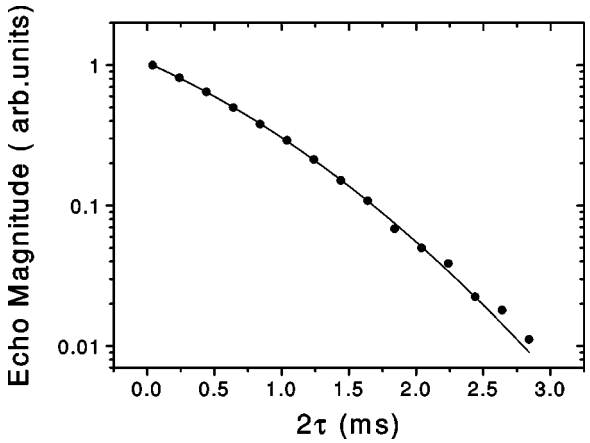

FIG. 12. Semi-logarithmic plot of the ^{63}Cu spin echo decays measured at a shift of 170 kHz (Fig. 10) of the $CuZr_2$ reference sample spectrum. The relaxation times obtained from the fit of Eq. (11) to the data are: T_2=1.01(2) ms and T_{2G}=1.44(4) ms.

TABLE I. Calculated large cluster T_{2G} values for various AlZr alloys. The values are calculated according to Eq. (13).

Alloy	Al_3Zr DO_{22}	Al_3Zr L_{12}	Al_2Zr C_{14}	$AlZr_2$ C_{16}	$AlZr_3$ L_{12}	$ALZr_3$ $D0_{22}$
T_{2G}(ms)	0.38	0.39	0.25	2.5	1.5	1.0

ary experience smaller numbers of next neighbors and possess a larger T_{2G} than nuclei located in the middle of the cluster. In order to identify ordered regions and to estimate their possible size the calculations were started with relatively large clusters and subsequently the cluster size was incrementally reduced and the average T_{2G} from all nuclei was calculated.

The eligible compounds were preselected from the stoichiometry of the sample and the extraordinary long T_1 of the Al nuclei. The high Al and Zr content favours the formation of Al_xZr_y compounds and band structure calculations of binary AlZr compounds predict a gap in the DOS at the Fermi level[10] leading to the observed relatively long T_1. The existence of pure Al metallic regions is excluded from the T_{2G} of 1.50(2) ms that is significantly larger than the experimental value of T_{2G}=291 μs reported for pure Al metal powder.[36] Even small clusters of only a few Atoms can be excluded because the T_{2G} calculated for a cluster of 4 Al Atoms in a cubic cell with a distance of 2.8 Å yields a value of 630 μs, which is significantly smaller than the measured value. As shown in Table I the calculated Al T_{2G} for various AlZr alloy differ significantly from the experimental value outside the estimated uncertainty of 10%. A good agreement between the measured and the simulated T_{2G} in the as-quenched sample was only achieved for L_{12} $AlZr_3$ with a lattice constant of 4.374 Å[37] yielding a theoretical large cluster value of T_{2G} of 1.54 ms. Calculating the T_{2G} on $AlZr_3$ clusters with 5^3 elementary cells yields an average T_{2G} of 1.74 ms and for 7^3 elementary cells, equivalent to 30 Å, 1.68 ms.

Treating the contributions to T_{2G} from $|\pm 3/2\rangle$ and $|\pm 5/2\rangle$ states as static would enlarge the calculated T_{2G} value by a factor of 5.8 for Al. For Al_2Zr (Table I) this would lead to 1.45 ms. However, Al_2Zr has the hexagonal C14 structure and a considerable shift anisotropy is expected from this structure. This shift anisotropy should lead to a pronounced shoulder in the central peak of the Al NMR spectra, that, however, is not seen. Therefore, the presence of Al_2Zr is not favored. The presence of Al_3Zr is also unfavored because Al NMR spectra of well ordered tetragonal Al_3Zr are known[24] and are expected to possess a much broader central peak ($\approx$1 MHz) in case of introducing some disorder into the crystal lattice. T_{2G} for the cubic Al_3Zr structure yields $\approx$2.2 ms if enlarged by the factor of 5.8. This value is larger than the experimental one and has to be reduced by 30% to meet the experimental value. On the other hand, in case of the ^{63}Cu T_{2G} value only a small deviation of the calculated one exits from the experimental one, if the calculation is made according to Eq. (14). Therefore, with the assumption that this calculation is also suitable in case of Al, we favor the presence of cubic $L_{12}AlZr_3$.

The L_{12} structure is a cubic structure which appears at first to be in contradiction with the observed quadrupole interaction. However, the strongly broadened central transition (Fig. 4) indicates some disorder in the structure and disordered cubic structures possess quadrupole interactions with a distribution of the EFG tensors. Furthermore, the structure is assumed to exist only over a range of a few nm and, therefore, a distribution of quadrupole frequencies should arise due to distortion and shear effects at the boundaries of the $AlZr_3$ regions. A further argument for a distorted cubic-like structure is the symmetry of the ^{27}Al spectra together with the relatively low quadrupole frequency of 1.6 MHz. In amorphous alloys the Al nuclei should experience considerable deviations from cubic symmetry, and therefore, large values of the quadrupole constant especially if the surrounding atoms possess much different valences. Gaussian distribution of a relatively low quadrupole frequency dominated by lattice charges is in contradiction to a supposed amorphous Al environment.

In order to investigate the effect of disorder on the second moment the calculation were repeated by introducing the estimated standard deviation of the lattice positions estimated in Sec. III C into the simulated clusters by randomly displacing the Al nuclei from there average lattice positions. The T_{2G} was averaged from 100 runs. A Gaussian distribution with a standard deviation of 6% reduced the average T_{2G} value from 1.68 to 1.6 ms which is satisfactory if one takes into account that experimental values are in general smaller than theoretical ones. The effects in metallic Al[36] and in the $CuZr_2$ reference sample are about 10% (Sec. IV A). From this point of view it is reasonable to assume a medium-range ordered cubic L_{12} $AlZr_3$-like structure which can be estimated to be of the order of 30 Å. This estimated order should be understood as an average size, since a distribution of sizes should be present in glass-forming alloys.

After the crystallization the experimental ^{27}Al T_{2G} changes to 1.00(2) ms, which is in good agreement with values of T_{2G}=1.08 ms calculated for the hexagonal $D0_{19}$ $AlZr_3$ phase. However, care has to be taken in the interpretation of this change. This decreased T_{2G} might indicate a change from the cubic L_{12}-like structure into a hexagonal $D0_{19}$-like order. If this assumption holds true, a drastic change in the quadrupole interaction should be observed, because such a transition means a transition from a disordered cubic symmetry to a hexagonal symmetry. However, the quadrupole constant is only increased by 30% and the shape of the whole ^{27}Al spectrum remains nearly unchanged after the crystallization. Thus, it is more probable that the increase of the ^{27}Al second moment is due to a compression of the L_{12} $AlZr_3$-like order, as discussed in section (III C). A calculation of the lattice constant required for a T_{2G}=1.0 ms yields 3.850 Å. One may argue that increasing the second moment may also occur from a growing of the L_{12} $AlZr_3$-like regions during the crystallization. However, increasing the ordered regions should decrease the disorder within these regions. Hence, an increased second moment should be accompanied by a decreased quadrupole interaction. Assuming a slight compression of L_{12} $AlZr_3$-like regions is, therefore, more probable.

C. ^{63}Cu second moments

Calculating the ^{63}Cu second moment was done according to Eq. (14). The measured T_{2G} of 1.24(4) ms of the as-

quenched sample is close to the value calculated for $C11_b$ $CuZr_2$ of $T_{2G}=1.54$ ms and close to the value found in the $CuZr_2$ reference sample. Assuming $CuZr_2$ ordered regions is supported by conclusions of Eifert *et al.*[38] The widths of $^{63/65}$Cu NMR spectra in Zr_xCu_{1-x} amorphous alloys are of the same order as the widths of the ^{63}Cu spectra presented in this work, which are surprisingly small for a glassy compound. In glassy alloys one should expect large quadrupole interactions due to considerable deviations from cubic symmetry.[38] Consequently, relatively low quadrupole interactions together with the second moment calculations can be taken as a strong hint for $CuZr_2$-like ordered regions.

After the crystallization the second moment has totally changed and is covered by the spin-spin relaxation time $T_2=0.5$ ms. In Sec. III G a value of T_{2G} of 7 ms was estimated for the Cu after the crystallization and confirmed by the spin-spin relaxation curve recorded at 30 K.

A structure calculation can hardly be done without knowledge of the possible quasicrystal structures, i.e., the Cu nuclei distances within these structures. However, the strongly enlarged T_{2G} is a clear proof for a structural change. Estimating the lattice constants of the $C11_b$ structure necessary for a T_{2G} of 7 ms yields values of a $a \approx 5.8$ Å and $b \approx 20$ Å which means an enlargement of the lattice constants by a factor of approximately 1.8. Such an enlargement cannot be explained with the assumption of a preserved $C11_b$ $CuZr_2$ structure.

V. SUMMARY

The presence of two medium-range orders is strongly indicated in an as-quenched $Zr_{59}Cu_{20}Al_{10}Ni_8Ti_3$ metallic glass by investigating and simulating the second moments of ^{27}Al and ^{63}Cu. The simulations for ^{27}Al second moments show best agreement with a L_{12} $AlZr_3$-like structure. The size of medium-range order can be estimated to be of the order of 30 Å. For Cu best agreement is achieved with a $C11_b$ $CuZr_2$-like structure.

The sample heated up to the first crystallization peak shows remarkable changes in the intensity of the ^{63}Cu NMR spectrum and the ^{63}Cu second moment. An increase of the amount of ^{63}Cu visible in the spectrum from 12% to nearly 100% can be recorded, with respect to the intensity of the ^{27}Al central transition. This intensity increase is accompanied by a strong decrease of the ^{63}Cu second moment. All these changes coincide with the occurrence of icosahedral order in the x-ray diffraction patterns after the annealing procedure and are the proof for the involvement of Cu into the quasicrystal. For the ^{27}Al spectra and second moments only relatively smooth variations are detectable after the crystallization. The second moment is increased by 50% and the quadrupole constant is also increased by nearly the same amount. The shape of the ^{27}Al NMR spectrum is nearly unchanged by the crystallization. A transformation from the L_{12} $AlZr_3$ phase to the $D0_{19}$ phase is improbable because a change from a disordered cubic structure to a tetragonal structure should increase the quadrupole constant abundantly clear by more than 30%. From this point of view it is more reasonable to assume a reduction of the L_{12} $AlZr_3$ lattice constants due to the quasicrystal formation. The quasicrystal requires more space in the sample than its approximants. This may explains the quasicrystal formation dependency on the Ti amount which is a discursive point in crystallography. Further investigations on samples with various Ti amounts are under progress.

ACKNOWLEDGMENTS

This work is supported by Deutsche Forschungsgemeinschaft (Grant Nos. Ec 111/10-1/2 and Lu 217/17-1/2).

*Electronic mail: breitzke@physik.fu-berlin.de
†Present address: TU Darmstadt, FB 11 Material- und Geowissenschaften, FG Physikalische Metallkunde, Petersenstrasse 23, D-64287 Darmstadt, Germany.

[1] A. Inoue, Acta Mater. **48**, 277 (2000).
[2] W. L. Johnson, *Bulk Glass-Forming Alloys: Science and Technology* (MRS Bulletin, 1999).
[3] U. Kühn, J. Eckert, N. Mattern, and L. Schultz, Appl. Phys. Lett. **77**, 3176 (2000).
[4] X.-P. Tang, J. F. Löffler, W. L. Johnson, and Y. Wu, J. Non-Cryst. Solids **317**, 118 (2003).
[5] U. Köster, J. Meinhardt, R. Roos, and H. Liebertz, Appl. Phys. Lett. **69**, 179 (1996).
[6] J. Eckert, N. Mattern, M. Zinkevitch, and M. Seidel, Mater. Trans., JIM **39**, 623 (1998).
[7] A. Inoue, T. Chan, M. W. Chen, T. Sakurai, J. Saida, and M. Matsushita, J. Mater. Res. **15**, 2195 (2000).
[8] L. Q. Xing, J. Eckert, W. Löser, and L. Schultz, J. Mater. Res. **74**, 664 (1999).
[9] W. Hoffmann, M. Baenitz, K. Lüders, A. Gebert, J. Eckert, and L. Schultz, Mater. Res. Soc. Symp. Proc. **554**, 95 (1999).
[10] P. Ravindran and R. Asokamani, Phys. Rev. B **50**, 668 (1994).
[11] A. Shastri, F. Borsa, D. R. Torgeson, J. E. Shield, and A. I. Goldman, Phys. Rev. B **50**, 15651 (1994).
[12] P. A. Bancel, P. A. Heiney, P. W. Stephens, A. I. Goldman, and P. M. Horn, Phys. Rev. Lett. **54**, 2422 (1985).
[13] X.-P. Tang, R. Busch, W. L. Johnson, and Y. Wu, Phys. Rev. Lett. **81**, 5358 (1998).
[14] T. Apih, M. Klanjšek, D. Rau, and J. Dolinšek, Phys. Rev. B **61**, 11213 (1999).
[15] T. J. Rowland, Phys. Rev. **119**, 900 (1960).
[16] W. Kohn and S. H. Vosko, Phys. Rev. **119**, 912 (1960).
[17] C. P. Slichter, *Principles of Magnetic Resonance*, 3rd ed. (Springer-Verlag, New York, 1990).
[18] A. Abragam, *The Principles of Nuclear Magnetism* (Oxford University Press, 1973).
[19] P. C. Taylor and P. J. Bray, J. Magn. Reson. (1969-1992) **2**, 305 (1970).
[20] P. C. Taylor, J. F. Baugher, and H. M. Kriz, Chem. Rev. (Washington, D.C.) **75**, 203 (1975).
[21] M. Bak, J. T. Rasmussen, and N. C. Nielsen, J. Magn. Reson. **147**, 296 (2000).

[22] D. R. Torgeson and R. G. Barnes, Phys. Rev. **136**, 738 (1964).
[23] D. Pines, *Solid State Physics*, Vol. 1 (Academic, New York, 1955).
[24] T. J. Bastow, C. T. Forwood, M. A. Gibson, and M. E. Smith, Phys. Rev. B **58**, 2988 (1998).
[25] C.-S. Lue, S. Chepin, J. Chepin, and J. H. Ross, Jr., Phys. Rev. B **57**, 7010 (1998).
[26] R. Kubo, J. Phys. Soc. Jpn. **6**, 975 (1962).
[27] E. R. Andrew and D. P. Tunstall, Proc. Phys. Soc. London **78**, 1 (1961).
[28] A. Narath, Phys. Rev. **179**, 359 (1969).
[29] A. Narath, Phys. Rev. **162**, 320 (1967).
[30] J. Korringa, Physica (Utrecht) **16**, 601 (1950).
[31] I. Bakonyi, H. E. Schone, L. K. Varga, K. Tompa, and A. Lovas, Phys. Rev. B **33**, 5030 (1986).
[32] J. Hafner, S. S. Jaswal, M. Tegze, A. Pflugi, J. Krieg, P. Oelhafen, and H. J. Guentherodt, J. Phys. F: Met. Phys. **18**, 2583 (1988).
[33] Yutaka Itoh, Hiroshi Yasuoka, Yoko Fujiwara, Yutaka Ueda, Takato Machi, Izumi Tomeno, Keishi Tai, Naoki Koshizuka, and Syoji Tanaka, J. Phys. Soc. Jpn. **61**, 1287 (1992).
[34] Atsushi Goto, W. G. Clark, Patrik Vonlanthen, Kenji B. Tanaka, Tadashi Shimizu, Kenjiro Hashi, P. V. P. S. S. Sastry, and Justin Schwartz, Phys. Rev. Lett. **89**, 127002 (2002).
[35] N. J. Curro and C. P. Slichter, J. Magn. Reson. **130**, 186 (1998).
[36] P. L. Sagalyn and A. Hofmann, Phys. Rev. **127**, 68 (1962).
[37] W. P. Pearson, *A Handbook of Lattice Spacing and Structures of Metals and Alloys* (Pergamon, New York, 1958).
[38] H.-J. Eifert, B. Elschner, and K. H. J. Buschow, Phys. Rev. B **25**, 7441 (1982).